Journal of African Earth Sciences 197 (2023) 104771

Contents lists available at ScienceDirect

Journal of African Earth Sciences

journal homepage: www.elsevier.com/locate/jafrearsci

Modeling the atmospheric dispersion of SO_2 from Mount Nyiragongo

Ronald Opio [a,*], Isaac Mugume [a,b], Joyce Nakatumba-Nabende [c], Michael Mbogga [d]

[a] Department of Geography, Geo-informatics and Climatic Sciences, Makerere University, Kampala, 7062, Uganda
[b] Directorate of Forecasting Services, Uganda National Meteorological Authority, Kampala, 7025, Uganda
[c] Department of Computer Science, Makerere University, Kampala, 7062, Uganda
[d] Department of Forestry, Biodiversity and Tourism, Makerere University, Kampala, 7062, Uganda

ARTICLE INFO

Keywords:
Nyiragongo
Sulphur dioxide
WRF-Chem
Deep learning
Africa

ABSTRACT

Mount Nyiragongo, an active volcano, is the most dominant natural source of sulphur dioxide (SO_2) in Africa. While a number of studies have employed atmospheric models to simulate the dispersion of SO_2 from this mountain, prior to this study, no attempt has been made to use deep learning to bias correct the model's estimates. Here, the Weather Research and Forecasting model coupled with chemistry (WRF-Chem) was used to simulate massive SO_2 plumes degassed from this mountain between September 2014 and August 2015. Satellite observations by the Ozone Monitoring Instrument (OMI) showed that the SO_2 spread to over 500 km from the volcano site. A deep convolutional autoencoder algorithm (WRF-DCA) was then applied to reduce the bias that WRF-Chem showed against the OMI observations. Finally, the correction performance of WRF-DCA was compared with a conventional bias correction method, linear scaling (WRF-LS). The performance of WRF-Chem, WRF-DCA, and WRF-LS was analyzed using three metrics, that is, the normalized mean bias (NMB), the root mean square error (RMSE), and Pearson's correlation coefficient (R). The results showed that WRF-Chem overestimated SO_2 at locations near the volcano site and underestimated SO_2 at locations further away from the volcano site. It generated an overall average NMB of −0.61 against the OMI observations. Respectively, WRF-DCA and WRF-LS reduced this bias by an average of 0.25 (40.9%) and 0.21 (34.4%). Furthermore, although both methods also reduced the RMSE and improved the correlation, WRF-DCA consistently performed better than WRF-LS. This study demonstrates the advantage that deep learning can provide in estimating volcanic SO_2 emissions.

1. Introduction

Sulphur dioxide (SO_2) is an atmospheric chemistry species that has been placed on the global environment watch list because of its association with air pollution, ecosystem damage and climate change (Aas et al., 2019; Theys et al., 2019). It is considered one of the principal air pollutants that has contributed to premature deaths and respiratory illnesses globally (Orellano et al., 2021). It also contributes to the deterioration of water, plant, and soil ecosystems by forming sulphuric acid (Grennfelt et al., 2020). SO_2 is also a short-lived climate forcing agent. It is a precursor to sulphate aerosols which influence the radiation budget by causing a cooling effect (Szopa et al., 2021). SO_2 also has a high spatial and temporal variability because of its short atmospheric residence time, which, in the troposphere, is in the order of days (Szopa et al., 2021). When SO_2 is emitted into the troposphere, its main removal pathway is through gas phase oxidation by the OH radical and liquid phase oxidation by H_2O_2. The latter happens inside cloud droplets and forms sulphate aerosols (Jacob, 2021; Von Schneidemesser et al., 2015). The reaction sequence is shown in equations (1)–(5) below.

$$SO_2 + OH \xrightarrow{M,H_2O} H_2SO_4 \quad (1)$$

$$SO_2(g) \rightleftarrows SO_2 \bullet H_2O \quad (2)$$

$$SO_2 \bullet H_2O \rightleftarrows HSO_3^- + H^+ \quad (3)$$

$$H_2O_2(g) \rightleftarrows H_2O_2(aq) \quad (4)$$

$$HSO_3^- + H^+ + H_2O_2(aq) \rightarrow SO_4^{2-} + 2H^+ + H_2O \quad (5)$$

The variability of SO_2 has been successfully monitored on a global scale over multiple decades using satellite instruments. These are; the Total Ozone Mapping Spectrometer (TOMS) (Krueger, 1983), the Global

* Corresponding author.
E-mail address: opioronald123@gmail.com (R. Opio).

https://doi.org/10.1016/j.jafrearsci.2022.104771
Received 18 July 2022; Received in revised form 14 October 2022; Accepted 19 October 2022
Available online 22 October 2022

Ozone Monitoring Experiment (GOME) (Eisinger and Burrows, 1998), the Scanning Imaging Absorption Spectrometer for Atmospheric Chartography (SCIAMACHY) (Bovensmann et al., 1999), the Ozone Monitoring Instrument (OMI) (Levelt et al., 2006, 2018), GOME-2 (Callies et al., 2000; Munro et al., 2016; Nowlan et al., 2011) and the most recent of them, the TROPOspheric Monitoring Instrument (TROPOMI) (Theys et al., 2019; Veefkind et al., 2012).

In Africa, SO_2 is emitted from both anthropogenic and natural sources. The dominant anthropogenic source is the combustion of sulphur-rich fossil fuels, for example, at the coal-fired power plants in South Africa (Shikwambana et al., 2020). The dominant natural source is the volcanic activity at Mt. Nyiragongo, located near the border separating the Democratic Republic of Congo and Rwanda. It is an active volcano that has the largest constant lava lake in the world located at its summit, and SO_2 is continuously degassed from it throughout the year (Dingwell et al., 2016; Pouclet and Bram, 2021). Consequently, the region around this mountain suffers the highest SO_2 pollution than any other region within East and Central Africa as shown in Fig. 1a. This problem of SO_2 degassing is further magnified whenever a volcanic eruption occurs. The most recent eruption occurred on May 22, 2021, and it produced more than 15 Dobson Units (DU) of SO_2 pollution (Opio et al., 2021). These two dominant sources of SO_2 have been shown in Fig. 1a.

This study focused on the region around Mt. Nyiragongo as the study site (Fig. 1b). In addition to the persistent SO_2 pollution over its atmosphere and threats of eruption from the mountain, this region also suffers from political unrest because of the presence of armed militia in the area (Lisa et al., 2021). This ongoing crisis makes it difficult to monitor SO_2 pollution using ground stations, thus satellite observations can be a suitable alternative, most especially because they also offer the advantage of tracking the full extent of the SO_2 plume. This study used observations made by OMI from 2005 to 2020. This period does not have any eruption event occurring within it, and was therefore dominated by passive degassing SO_2 emissions other than eruptive emissions. The SO_2 observations during this period were analyzed to identify the peak period, which was then used as the target study period for numerical modeling.

There are limited studies that have applied numerical modeling to study the SO_2 pollution from Mt. Nyiragongo. For example, on a global scale, Lamotte et al. (2021) used the MOCAGE (Modèle de Chimie Atmosphérique à Grande Échelle) chemistry transport model to study the contribution of degassed SO_2 from Mt. Nyiragongo and other mountains to the global sulphur budget. Their evaluation was made against OMI SO_2 observations. On a local scale, Landgren (2011) and Dingwell et al. (2016) used the FLEXPART-WRF model to study the dispersion of SO_2 from this mountain. Both of them compared their simulations to observations taken by ground based Differential Optical Absorption Spectroscopy (DOAS) instruments. These local-scale studies had a small geographical coverage of less than 300 km from the volcano site. By contrast, this study simulated much larger SO_2 plumes that spread to over 500 km from the volcano site. For this, the present study used the Weather Research and Forecasting model coupled with chemistry (WRF-Chem). This is the first time that WRF-Chem is used to simulate degassed SO_2 emitted from Mt. Nyiragongo. The first purpose of this study was thus to evaluate the performance of WRF-Chem.

Further, an autoencoder based on a deep convolutional neural network was applied to correct the bias that WRF-Chem showed when evaluated against the OMI observations. This study is also the first attempt to use deep learning to bias correct WRF-Chem estimates of SO_2 emitted from Mt. Nyiragongo. The second purpose of this study was thus to evaluate the performance of WRF-Chem when bias corrected using the autoencoder. In the rest of the article, the WRF-Chem output corrected with the autoencoder is referred to with the acronym WRF-DCA. Furthermore, in order to give a comprehensive performance analysis of WRF-DCA, it was compared to the linear scaling technique as a benchmark (Fang et al., 2015). This is a popular bias correction technique because it has modest data requirements and is relatively simple to implement. In the rest of the article, the WRF-Chem output corrected using linear scaling is referred to with the acronym WRF-LS.

2. Data and methods

2.1. SO_2 observations

Observations of the vertical column density (VCD) of SO_2 were obtained from the Ozone Monitoring Instrument (OMI) (Li et al., 2020). It's a spectrometer aboard NASA's Aura satellite which has been making observations of SO_2 and other trace gases since July 2004. The observations are made daily at a resolution of 13 × 24 km^2 at nadir (Levelt et al., 2006, 2018). The retrieval algorithm is based on principal component analysis (Li et al., 2013). This study utilized the total column SO_2 product that is provided at a resolution of $0.25^0 \times 0.25^0$ (~27.5 km) via the Goddard Earth Sciences Data and Information Services Center (GES DISC).

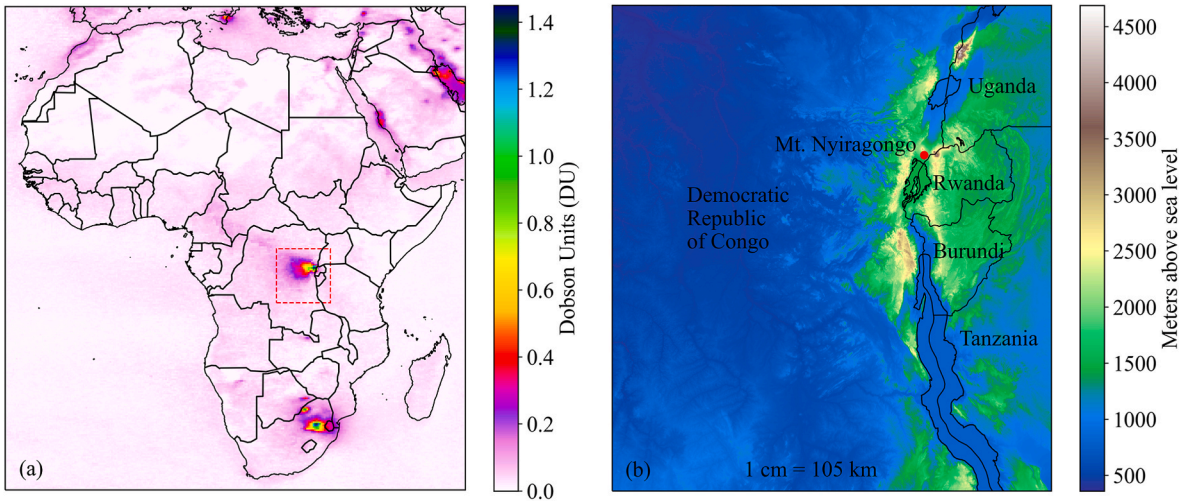

Fig. 1. (a) Map of Africa showing the long term (2005–2020) average SO_2 vertical column density as observed by OMI. The two dominant sources, Mt. Nyiragongo and the power plants in South Africa clearly standout. The dashed red box is the simulation domain used in this study. (b) Terrain of the study domain. The red dot is the location of Mt. Nyiragongo.

2.2. Wind data

Zonal and meridional wind components for the study domain were obtained from ERA5 reanalysis (Hersbach et al., 2020). This is the 5th generation reanalysis dataset produced by the European Centre for Medium Range Weather Forecasts (ECMWF). This study used winds at 600 hPa height. This is ~4 km and it is the closest available pressure level above the volcano's summit for which wind data is provided. The data were downloaded from the Copernicus Climate Data Store as monthly averages at a spatial resolution of $0.25^0 \times 0.25^0$ (~27.5 km).

2.3. WRF-Chem model setup and data inputs

Version 4.3 of the Weather Research and Forecasting model coupled with chemistry (WRF-Chem) was utilized for making the simulations of the SO_2 concentration degassed from the volcano. WRF-Chem's framework is an online integrated coupling between a meteorological model and a chemical transport model. Both meteorology and chemistry variables are thus simulated on the same grid and over the same time steps and the feedbacks between the two components are also catered for (Grell et al., 2005).

The meteorological model is the WRF modeling system which uses the Advanced Research WRF (ARW) dynamical core. It is a non-hydrostatic model which performs numerical integration on staggered Arakawa C-grid with 2nd and 3rd order Runge-Kutta time integration. The model can use either a terrain-following vertical coordinate which has constant pressure at the model top or a hydrostatic pressure coordinate which is terrain-following near the surface (Skamarock et al., 2019). The ARW solver also has a variety of parameterization options available to describe cumulus activity, cloud microphysics, radiation, and boundary layer changes among others. The options selected for this study are summarized in Table 1. The meteorological initial and boundary conditions were obtained from the National Centers for Environmental Prediction (NCEP) Final (FNL) Operational Global Analysis data (NCEP, 2000) at a spatial resolution of $1^o \times 1^o$ (~110 km) and a 6-hourly temporal resolution.

The chemistry module attached to the WRF handles the chemical emissions of gases and aerosols, their transport, dispersion and deposition (Grell et al., 2005). The module has only one chemistry option for simulating SO_2 concentration, that is, option 402 and it was the one used for this study. Furthermore, version 1.5 of the PREP-CHEM-SRC tool (Freitas et al., 2011) was used to generate the volcanic emissions data for WRF-Chem. These emissions are generated using data from the Aerosol Comparisons between Observations and Models (AEROCOM) program. It contains data for both eruptive and non-eruptive volcanic SO_2 daily emission rate (kg m^{-2} dy^{-1}) along with other variables such as the volcano's name, height above sea level, plume height, longitude and latitude. The data are available from January 1979 to December 2010 for all the volcanoes listed in the Global Volcanism Program database that is maintained by the Smithsonian Institute. The WRF-Chem simulations of 2009 and 2010 were done with their corresponding emissions while the simulations of 2011–2015 were done using 2010 emissions since they were the most recent. The SO_2 VCD from WRF-Chem were obtained by integrating vertically for all model layers from the surface up to the model top at 50 hPa. The final SO_2 VCD was thus obtained in Dobson Units (DU), where 1 DU = 2.69×10^{16} molecules/cm^2.

Table 1
WRF-Chem model setup.

Model Set-up	Value
Model version	4.3
Domain	1 domain (see Fig. 1)
Simulation period	Monthly runs from September 2009 to August 2015
Model spin-up period	1 day
Horizontal resolution	10×10 km^2
Vertical resolution	35 eta levels up to 50 hPa
Domain size	100×100 grids (longitude $\times$ latitude)
Meteorological boundary	NCEP FNL reanalysis (110 km, 6-hourly)
Physics option	**Adopted scheme**
Microphysics	Lin et al. (Lin et al., 1983)
Cumulus parameterization	Grell 3-D (Grell and Dévényi, 2002)
Shortwave radiation	Rapid Radiative Transfer Model for GCMs (RRTMG) (Iacono et al., 2008)
Longwave radiation	Rapid Radiative Transfer Model for GCMs (RRTMG) (Iacono et al., 2008)
Land surface	Noah land surface model (Chen and Dudhia, 2001)
Planetary boundary layer	Yonsei University scheme (Hong et al., 2006)
Chemistry option	**Adopted scheme**
Option 402	Volcanic ash fall and SO_2 concentration

2.4. Data control

The OMI SO_2 data were regridded from $0.25^0 \times 0.25^0$ (~27.5 km) to $0.1^0 \times 0.1^0$ (~10 km) to match the WRF-Chem grid. The interest was to retain the higher resolution option as this would be profitable for training WRF-DCA. The OMI SO_2 data used were thus at a resolution of $0.1^0 \times 0.1^0$.

2.5. Setup of the convolutional autoencoder model

The convolutional autoencoder model applied in this study had two parts; the encoding part and the decoding part (Fig. 2). The encoding part had five convolutional layers (Conv1 to Conv5) with a rectified linear unit (ReLU) (Nair and Hinton, 2010) as the activation function. All the layers used 3×3 filters which varied in number. Conv1 had 32 filters, and these doubled with each subsequent step such that Conv5 had 512 filters. Each convolution layer was also followed by a 2×2 max pooling operation. The end result of the encoding process is a compressed version of the image, which then goes through the decoding process. The decoding part of the algorithm is made up of deconvolution layers with ReLU functions. It's arranged in an order that mirrors the encoding arm such that it restores the image back to its original dimension.

Paired images of the model output and the corresponding observations were fed into the algorithm, which then learnt the representation of the two images and their differences. The images fed in had a size of 96×96 pixels. The data used for training the algorithm is described in section 3.1. The training process used 250 training iterations (epochs) and a batch size of 3. The model was compiled in Python 3.9.7 using the Keras deep learning library (Chollet, 2015) with Adam optimization (Kingma and Ba, 2014) and the mean squared error as the loss function. The code has been deposited on GitHub.[1] The total training time taken was 12.5 min on a 7th generation Intel Core i5-7200U processor clocked at 2.5 GHz. The final validation mean squared error was 0.0032.

2.6. Description of the linear scaling technique

This is a popular linear technique that has been applied to bias correct a variety of regional climate models (Fang et al., 2015; Jakob Themeβl et al., 2011; Lafon et al., 2013; Teng et al., 2015). In some literature such as Han et al. (2021) it is also referred to as anomaly correction with observations. In this work, the LS method has been adapted to handle spatial data. For each grid cell (i, j), the historical mean for the model simulations, $\overline{S_{i,j}}$ and the observations, $\overline{O_{i,j}}$ were calculated as shown in equations (6) and (7). These calculations were done with the same historical data used for training the autoencoder algorithm. The bias corrected model values for the test period, $S^*_{i,j}$ were

[1] https://github.com/Opio-Cornelius/analysis_volcanic_emissions.

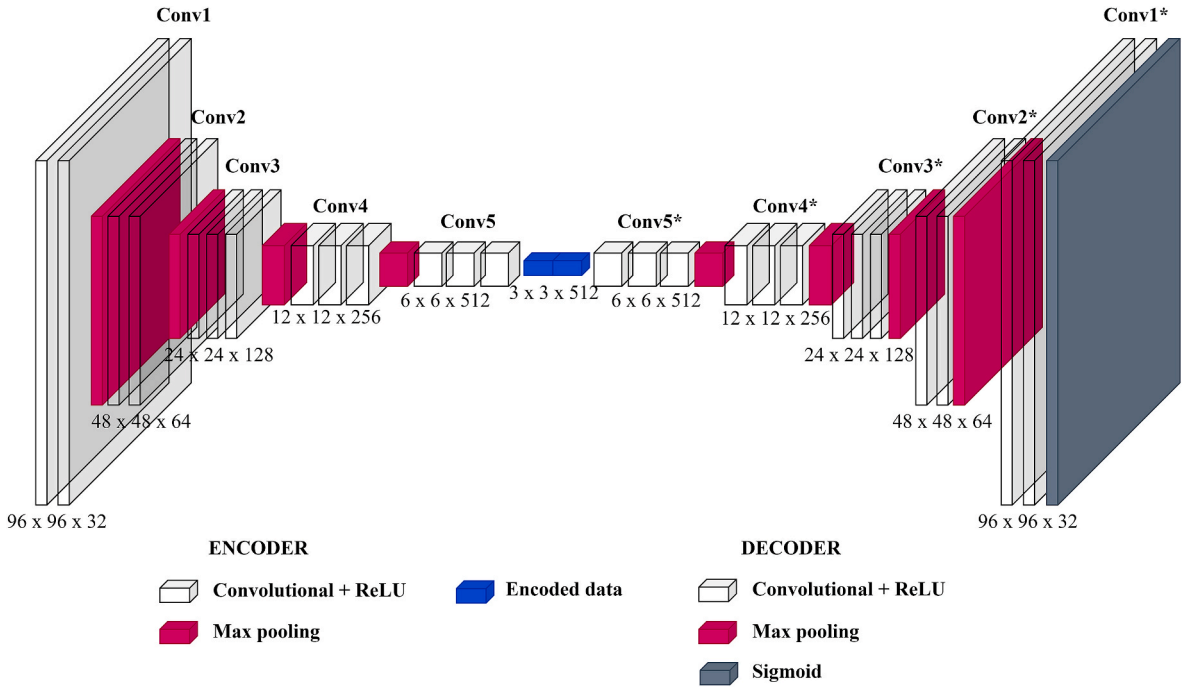

Fig. 2. Structure of the deep convolutional autoencoder used. The asterisk (*) sign marks the deconvolution layers.

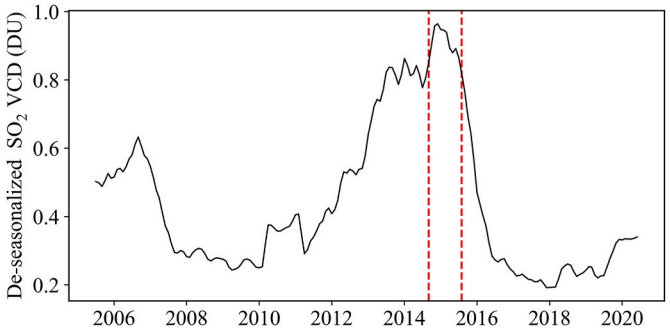

Fig. 3. De-seasonalized timeseries of area-averaged SO_2 VCD from 2005 to 2020. The period demarcated with vertical dashed red lines is the simulation period selected for this study.

then calculated as shown in equation (8). All the data were fed in on a monthly basis.

$$\overline{S_{i,j}} = \frac{1}{n}\sum S_{i,j} \tag{6}$$

$$\overline{O_{i,j}} = \frac{1}{n}\sum O_{i,j} \tag{7}$$

$$S^{*}_{i,j} = S_{i,j} + \left(\overline{O_{i,j}} - \overline{S_{i,j}}\right) \tag{8}$$

2.7. Evaluation metrics

Three evaluation metrics were used to assess the performance of the WRF-Chem, WRF-LS and WRF-DCA. These were; the root mean squared error (RMSE), the normalized mean bias (NMB) and Pearson's correlation coefficient (R). These methods have been described with adequate detail in Ivatt and Evans (2020).

3. Results

3.1. Timeseries analysis

A timeseries decomposition was done on the 16-year data record of SO_2 data taken for the pixels around the volcano site. The results showed that the most outstanding peak period of degassed SO_2 emissions from the volcano were from September 2014 to August 2015. All the 12 months in this period had above 0.84 DU of SO_2. This was the test period selected for modeling SO_2 using WRF-Chem. There were, however, other much weaker peaks observed in the series, in September 2006, April 2010, March 2011 and from January to June of 2014. Furthermore, in order to apply the WRF-DCA algorithm, it had to be trained and validated on data that does not overlap with the test period. For this, WRF-Chem simulations and observation data were obtained for the period from September 2009 to August 2014, these were 60 months. Of these data, 48 months (September 2009 to August 2013) were used for training and 12 months (September 2013 to August 2014) were used for validation.

3.2. Simulations of SO_2

Fig. 4 compares the spatial distribution of the SO_2 VCD based on seasonal averages. OMI observations show that majority of the SO_2 shifts westward from the volcano site into DRC. Higher SO_2 amounts between 1 and 4 DU were majorly present in the DJF, MAM and JJA seasons. Smaller SO_2 amounts below 1 DU were observed throughout all the seasons and they spread much further from the volcano site. WRF-Chem correctly simulated the westward spread of SO_2 although with a much smaller spatial coverage. The simulated SO_2 between 1 and 4.5 DU was concentrated close to the volcano site while SO_2 amounts below 1 DU were spread further away. This consequently generated an overestimation bias of more than 2 DU at the volcano site and an underestimation bias of between 0.1 and 3.5 DU in the areas further away from the volcano site. WRF-LS reduced both the underestimation and overestimation bias by about 1 DU. This was the systematic bias that was present in the simulations for all the four seasons. In comparison, WRF-DCA removed between 1 and 2 DU of underestimation bias over DRC

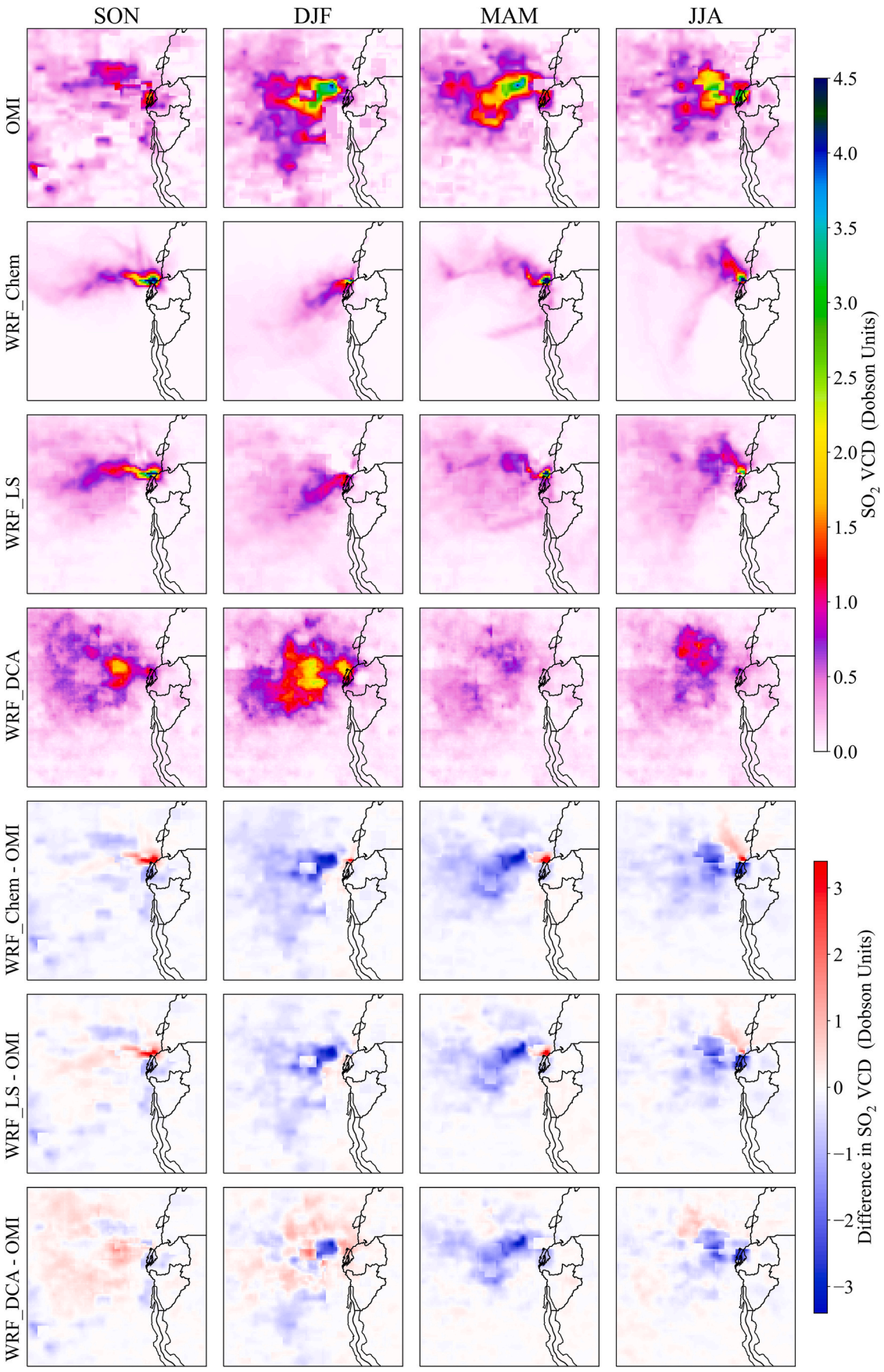

Fig. 4. Spatial patterns and differences between observed and modelled SO_2 VCD over the study area. Patterns have been organized by seasons; September to November (SON), December to February (DJF), March to May (MAM), and June to August (JJA).

and about 2 DU of overestimation bias close to the volcano site. However, during the SON, DJF and JJA seasons, WRF-DCA also generated a slight overestimation bias of about 1 DU over some parts of DRC. This overestimation was not present in the WRF-Chem output.

The temporal variation (Fig. 5) also shows that WRF-Chem underestimated the SO_2 VCD throughout the year. Its average NMB was −0.61. WRF-LS reduced this by an average of 0.21 (34.4%). The bias reduction happened in each of the months except October. By contrast, WRF-DCA reduced the NMB by an average of 0.25 (40.9%) and it had the best bias reduction for 10 of the 12 months. These were all other months except for October and April. WRF-DCA also never achieved a bias reduction in October.

WRF-Chem generated an average RMSE of 0.56 DU. WRF-LS had lower RMSE compared to WRF-Chem for all the months. It reduced the RMSE by an average of 0.06 DU (10.7%). By contrast, WRF-DCA had lower RMSE compared to WRF-Chem for 10 months, that is, all other months except October and January. Overall, WRF-DCA reduced the RMSE by an average of 0.1 DU (17.8%). Fig. 6 further shows that WRF-LS and WRF-DCA make improvements to the correlation. Respectively for SON, DJF, MAM and JJA, WRF-LS increased the correlation by 0.13 (48.1%), 0.22 (46.8%), 0.31 (155%) and 0.27 (79.4%) while WRF-DCA increased it by 0.28 (103.7%), 0.22 (46.8%), 0.51 (255%) and 0.33 (97%).

4. Discussion

The results show that WRF-Chem overestimates the amount of SO_2 close to the volcano's vent. An earlier study by Dingwell et al. (2016) also found a similar overestimation bias. However, much further away from the volcano, WRF-Chem underestimates the SO_2 amount. An investigation of the wind speed and direction at 600 hPa height (Fig. 7) might offer one explanation to this. During the SON season, there is a large area west of the volcano where the wind slows down to less than 5 ms^{-1}. This was contrary to ERA5 which showed wind speeds above 5 ms^{-1} in that area. Further, during SON, DJF and MAM, the wind speeds below 5 ms^{-1} tend to converge and yet ERA5 reanalysis shows continued motion even at these speeds. This tendency to converge happens east of the volcano during SON and southwest of the volcano during DJF and MAM. The largest difference was during the JJA season. WRF-Chem had a southeasterly wind flow which was contrary to the easterly and northeasterly wind flow shown by ERA5. These conditions could have limited the dispersion of SO_2 in the WRF-Chem simulations. Fig. 8 shows that very low amounts of SO_2 got transported westward after longitude 28^0 E. Typically, this was less than 0.15 DU of SO_2 which was persistently lower than what was observed by OMI.

WRF-DCA's superior performance at reducing the NMB and RMSE and increasing the correlation could be related to the nonlinearity of the mathematical functions in the algorithm. They are able to alter second order moments, that is, the standard deviation and the variance of the data. In comparison, WRF-LS could only alter the first order moment, which is, the mean value (Lafon et al., 2013; Teng et al., 2015).

For the particular test case used here, WRF-DCA only achieved a moderate bias reduction since only 40.9% of the bias was removed. The high pollution event simulated here was the only one of such magnitude in the entire data series, therefore, the algorithm did not have sufficient comparable examples to learn from. For this reason, it's likely that even if this study had used all the available historical data from 2005 (Fig. 3), the algorithm would still not have improved in performance. By contrast, in test cases where sufficient event examples have been provided, such deep learning algorithms can achieve a bias reduction of more than 75%. See, for example Han et al. (2021), Le et al. (2020) and Tao et al. (2016).

5. Conclusion

Being able to predict the likely dispersion extent and characteristics of hazardous volcanic emissions is an important step in mitigating their impact on human health. This work demonstrates the application of numerical modeling to simulate the dispersion of volcanic SO_2 emissions. The WRF-Chem model was used to simulate large SO_2 plumes emitted by Mt. Nyiragongo from September 2014 to August 2015. The model showed a clear overestimation bias close to the volcano and an underestimation bias further away. There was also a deficiency in the dispersion of degassed SO_2 by WRF-Chem. One possible cause was shown to be the incorrect wind patterns above the volcano's summit. Wind speeds below 5 ms^{-1} showed a tendency to converge.

A deep convolutional autoencoder algorithm (WRF-DCA) was then applied to bias correct the WRF-Chem model output and its performance

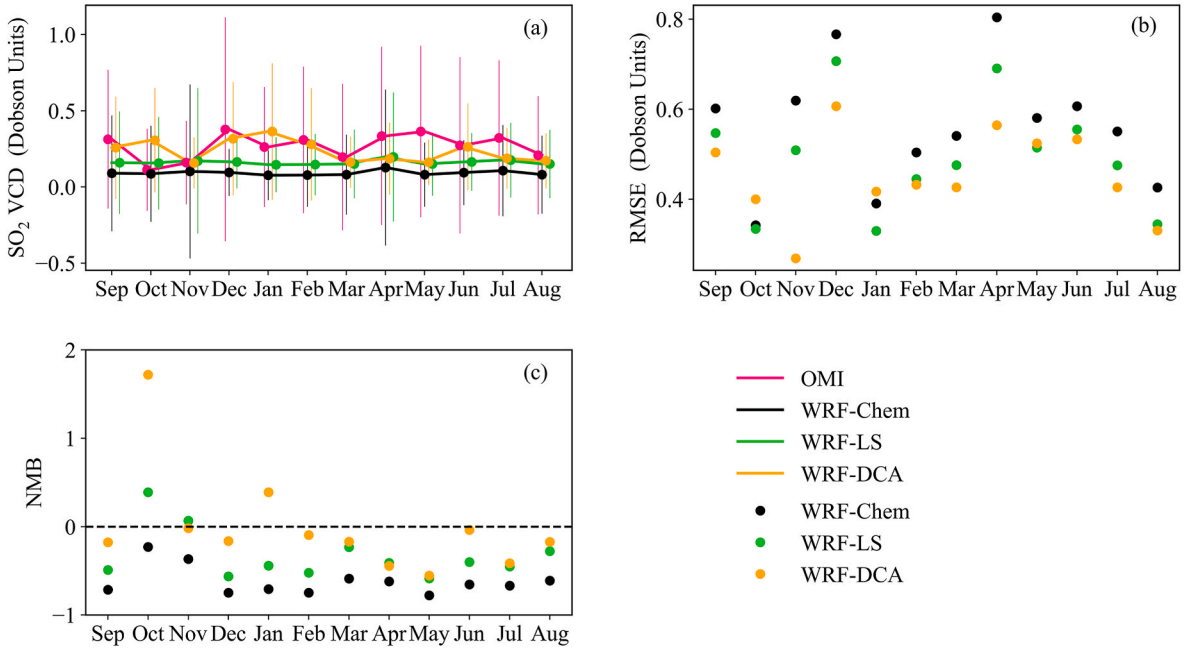

Fig. 5. Monthly comparisons between modelled and observed SO_2 VCD. (a) is the mean SO_2 VCD. The vertical bars are the standard deviations from the mean. (b) is the root mean square error (RMSE) and (c) is the normalized mean bias (NMB).

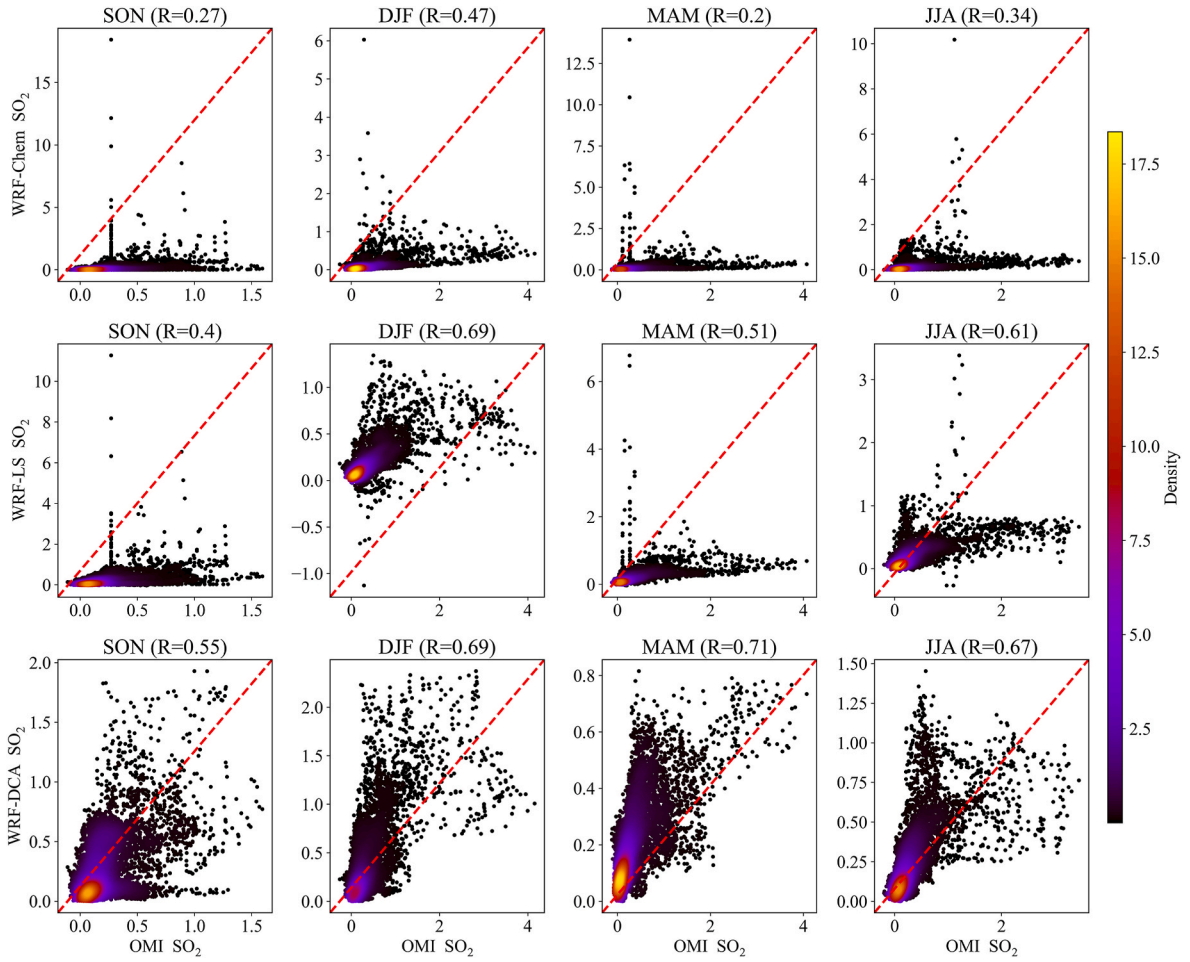

Fig. 6. Scatter plots with kernel density estimation and correlations for the SO_2 VCD (Dobson Units) of WRF-Chem, WRF-LS and WRF-DCA against OMI observations. The dashed red line is the 1:1 line.

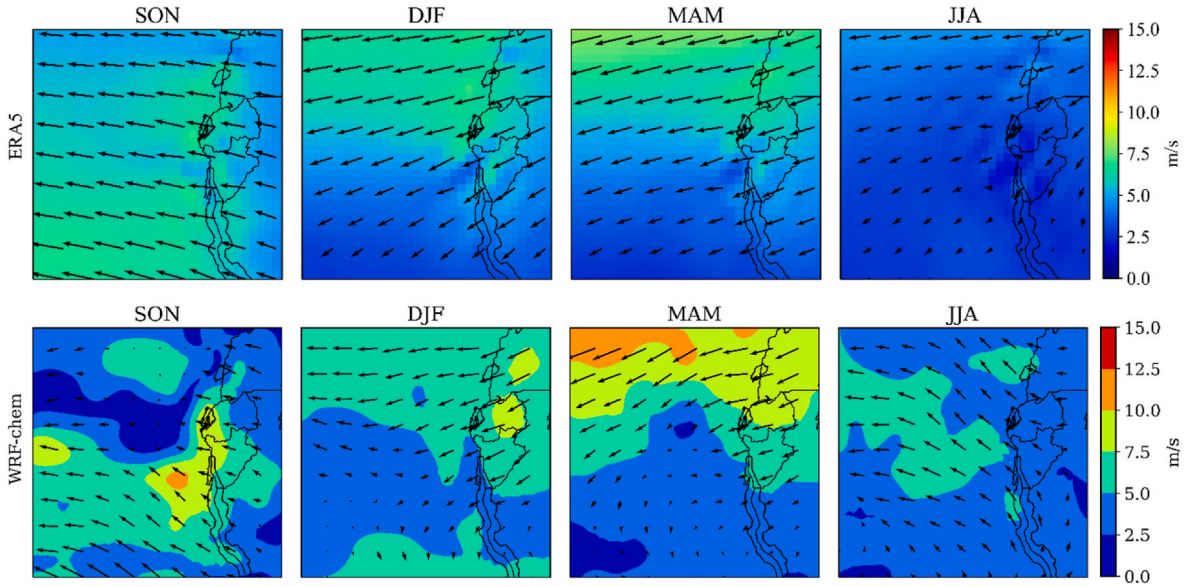

Fig. 7. 600 hPa wind speed and direction from ERA5 reanalysis and the WRF-Chem model.

was compared the conventional linear scaling method (WRF-LS). WRF-DCA achieved a bias reduction of 40.9% while WRF-LS achieved a reduction of 34.4%. WRF-DCA also had a lower RMSE and higher correlation compared to WRF-LS. This moderate performance of WRF-DCA is because the pollution event tested here was the only one of such magnitude that has so far been observed by OMI, therefore, this

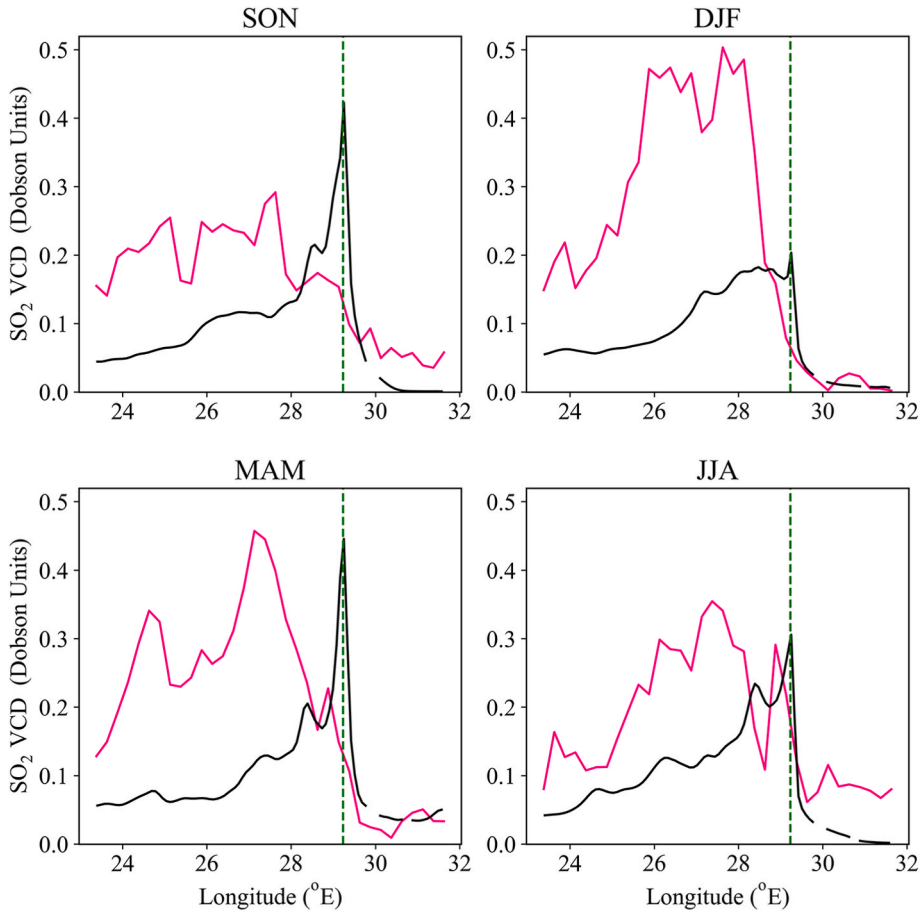

Fig. 8. Horizontal distribution of SO_2 across the domain as observed by OMI (pink lines) and as simulated by WRF-Chem (black lines). The dashed green lines show the location of Mt. Nyiragongo.

study could not provide sufficient examples for the algorithm to learn from. This method would perhaps show higher performance if applied to relatively lower SO_2 pollution episodes which happen often. This has not been demonstrated in this work.

WRF-Chem is a capable scientific tool for modeling volcanic emissions because it simulates the chemical concentrations along with the influence that meteorological conditions have on their dispersion. However, it suffers from bias arising partly from the limited range to which the species get dispersed. Egan (2019) has demonstrated that making some code modification could be one method to correct the dispersion deficiency. This study has also demonstrated that doing a bias correction based on historical data can also help improve the performance of WRF-Chem.

Declaration of competing interest

The authors declare that they have no known competing financial interests or personal relationships that could have appeared to influence the work reported in this paper.

Data availability

Data will be made available on request.

Acknowledgement

The authors wish to acknowledge that the funding for this work was provided by the International Development Research Centre (IDRC) and the Swedish International Development Cooperation Agency (SIDA) through the Artificial Intelligence for Development (AI4D) Africa programme that is managed by the African Center for Technology Studies (ACTS). The server cluster for running WRF-Chem was provided by the Uganda National Meteorological Authority (UNMA).

References

Aas, W., Mortier, A., Bowersox, V., Cherian, R., Faluvegi, G., Fagerli, H., Hand, J., Klimont, Z., Galy-Lacaux, C., Lehmann, C.M.B., Myhre, C.L., Myhre, G., Olivié, D., Sato, K., Quaas, J., Rao, P.S.P., Schulz, M., Shindell, D., Skeie, R.B., et al., 2019. Global and regional trends of atmospheric sulfur. Sci. Rep. 9 (1), 1–11. https://doi.org/10.1038/s41598-018-37304-0.

Bovensmann, H., Burrows, J.P., Buchwitz, M., Frerick, J., Noël, S., Rozanov, V.V., Chance, K.V., Goede, A.P.H., 1999. SCIAMACHY: mission objectives and measurement modes. J. Atmos. Sci. 56 (2), 127–150. https://doi.org/10.1175/1520-0469(1999)056<0127:SMOAMM>2.0.CO;2.

Callies, J., Corpaccioli, E., Eisinger, M., Hahne, A., Lefebvre, A., 2000. GOME-2 - Metop's Second-Generation Sensor for Operational Ozone Monitoring. ESA Bulletin. https://www.researchgate.net/profile/J-Callies/publication/285296960_GOME-2-Metop's_second-generation_sensor_for_operational_ozone_monitoring/links/5c7b9125a6fdcc4715a9ba5c/GOME-2-Metops-second-generation-sensor-for-operational-ozone-monitoring.pdf. January.

Chen, F., Dudhia, J., 2001. Coupling an advanced land surface–hydrology model with the penn state-NCAR MM5 modeling system. Part I: model implementation and sensitivity. Mon. Weather Rev. https://doi.org/10.1175/1520-0493(2001)129<0569:CAALSH>2.0.CO;2.

Chollet, F., 2015. Keras: the Python Deep Learning Library. https://keras.io.

Dingwell, A., Rutgersson, A., Claremar, B., Arellano, S., Yalire, M.M., Galle, B., 2016. Seasonal and diurnal patterns in the dispersion of SO2 from Mt. Nyiragongo. Atmos. Environ. 132, 19–29. https://doi.org/10.1016/j.atmosenv.2016.02.030.

Egan, S.D., 2019. Modelling Volcanic Ash and Sulfur Dioxide with the Weather Research Forecasting with Chemistry (WRF-Chem) Model. University of Alaska Fairbanks. http://hdl.handle.net/11122/10895.

Eisinger, M., Burrows, J.P., 1998. Tropospheric sulfur dioxide observed by the ERS-2 GOME instrument. Geophys. Res. Lett. 25 (22), 4177–4180. https://doi.org/10.1029/1998GL900128.

Fang, G.H., Yang, J., Chen, Y.N., Zammit, C., 2015. Comparing bias correction methods in downscaling meteorological variables for a hydrologic impact study in an arid area in China. Hydrol. Earth Syst. Sci. 19 (6), 2547–2559. https://doi.org/10.5194/hess-19-2547-2015.

Freitas, S.R., Longo, K.M., Alonso, M.F., Pirre, M., Marecal, V., Grell, G., Stockler, R., Mello, R.F., Sánchez Gácita, M., 2011. PREP-CHEM-SRC - 1.0: a preprocessor of trace gas and aerosol emission fields for regional and global atmospheric chemistry models. Geosci. Model Dev. (GMD) 4 (2), 419–433. https://doi.org/10.5194/gmd-4-419-2011.

Grell, G.A., Dévényi, D., 2002. A generalized approach to parameterizing convection combining ensemble and data assimilation techniques. Geophys. Res. Lett. 29 (14), 10–13. https://doi.org/10.1029/2002GL015311.

Grell, G.A., Peckham, S.E., Schmitz, R., Mckeen, S.A., Frost, G., Skamarock, W.C., Eder, B., 2005. Fully coupled "' online "' chemistry within the WRF model. Atmos. Environ. https://doi.org/10.1016/j.atmosenv.2005.04.027.

Grennfelt, P., Engleryd, A., Forsius, M., Hov, Ø., Rodhe, H., Cowling, E., 2020. Acid rain and air pollution: 50 years of progress in environmental science and policy. Ambio 49 (4), 849–864. https://doi.org/10.1007/s13280-019-01244-4.

Han, L., Chen, M., Chen, K., Chen, H., Zhang, Y., Lu, B., Song, L., Qin, R., 2021. A deep learning method for bias correction of ECMWF 24-240 h Forecasts. Adv. Atmos. Sci. 38 (9), 1444–1459. https://doi.org/10.1007/s00376-021-0215-y.

Hersbach, H., Bell, B., Berrisford, P., Hirahara, S., Horányi, A., Muñoz-Sabater, J., Nicolas, J., Peubey, C., Radu, R., Schepers, D., Simmons, A., Soci, C., Abdalla, S., Abellan, X., Balsamo, G., Bechtold, P., Biavati, G., Bidlot, J., Bonavita, M., et al., 2020. The ERA5 global reanalysis. Q. J. R. Meteorol. Soc. 146 (730), 1999–2049. https://doi.org/10.1002/qj.3803.

Hong, S.-Y., Noh, Y., Dudhia, J., 2006. A new vertical diffusion package with an explicit treatment of entrainment processes. Mon. Weather Rev. https://doi.org/10.1175/MWR3199.1.

Iacono, M.J., Delamere, J.S., Mlawer, E.J., Shephard, M.W., Clough, S.A., Collins, W.D., 2008. Radiative forcing by long-lived greenhouse gases: calculations with the AER radiative transfer models. J. Geophys. Res. Atmos. 113 (13), 2–9. https://doi.org/10.1029/2008JD009944.

Ivatt, P.D., Evans, M.J., 2020. Improving the prediction of an atmospheric chemistry transport model using gradient-boosted regression trees. Atmos. Chem. Phys. 20 (13), 8063–8082. https://doi.org/10.5194/acp-20-8063-2020.

Jacob, D.J., 2021. Introduction to Atmospheric Chemistry: Supplemental Questions and Problems, eleventh ed. Harvard University https://projects.iq.harvard.edu/files/acmg/files/edu_jacob_atmchem_problems_jan_2021.pdf.

Jakob Themeßl, M., Gobiet, A., Leuprecht, A., 2011. Empirical-statistical downscaling and error correction of daily precipitation from regional climate models. Int. J. Climatol. 31 (10), 1530–1544. https://doi.org/10.1002/joc.2168.

Kingma, D.P., Ba, J.L., 2014. Adam: A Method for Stochastic Optimization. ArXiv, 1-15. https://arxiv.org/abs/1412.6980.

Krueger, A.J., 1983. Sighting of El Chichón sulfur dioxide clouds with the Nimbus 7 total ozone Mapping spectrometer. Science 220 (4604), 1377–1379. https://doi.org/10.1126/SCIENCE.220.4604.1377.

Lafon, T., Dadson, S., Buys, G., Prudhomme, C., 2013. Bias correction of daily precipitation simulated by a regional climate model: a comparison of methods. Int. J. Climatol. 33 (6), 1367–1381. https://doi.org/10.1002/joc.3518.

Lamotte, C., Guth, J., Marécal, V., Cussac, M., Hamer, P.D., Theys, N., Schneider, P., 2021. Modeling study of the impact of SO2 volcanic passive emissions on the tropospheric sulfur budget. Atmos. Chem. Phys. 21 (14), 11379–11404. https://doi.org/10.5194/ACP-21-11379-2021.

Landgren, O., 2011. Implementation and Validation of a Meteorological Dispersion Model Applied on Volcanic Gas Emission for Studies of Environmental Impact. Chalmers University of Technology. https://odr.chalmers.se/handle/20.500.12380/165052.

Le, X.H., Lee, G., Jung, K., An, H.U., Lee, S., Jung, Y., 2020. Application of convolutional neural network for spatiotemporal bias correction of daily satellite-based precipitation. Rem. Sens. 12 (17) https://doi.org/10.3390/RS12172731.

Levelt, P.F., Joiner, J., Tamminen, J., Veefkind, J.P., Bhartia, P.K., Zweers, D.C.S., Duncan, B.N., Streets, D.G., Eskes, H., Van Der, R.A., McLinden, C., Fioletov, V., Carn, S., De Laat, J., Deland, M., Marchenko, S., McPeters, R., Ziemke, J., Fu, D., et al., 2018. The ozone monitoring instrument: overview of 14 years in space. Atmos. Chem. Phys. 18 (8), 5699–5745. https://doi.org/10.5194/acp-18-5699-2018.

Levelt, P.F., Van Den Oord, G.H.J., Dobber, M.R., Mälkki, A., Visser, H., De Vries, J., Stammes, P., Lundell, J.O.V., Saari, H., 2006. The ozone monitoring instrument. IEEE Trans. Geosci. Rem. Sens. 44 (5), 1093–1100. https://doi.org/10.1109/TGRS.2006.872333.

Li, C., Joiner, J., Krotkov, N.A., Bhartia, P.K., 2013. A fast and sensitive new satellite SO2 retrieval algorithm based on principal component analysis: application to the ozone monitoring instrument. Geophys. Res. Lett. 40 (23), 6314–6318. https://doi.org/10.1002/2013GL058134.

Li, C., Krotkov, N.A., Leonard, P., 2020. OMI/Aura sulfur dioxide (SO2) total column L3 1 day best pixel in 0.25 degree x 0.25 degree V3. In: Goddard Earth Sciences Data and Information Services Center. https://doi.org/10.5067/Aura/OMI/DATA3008 *(GES DISC)*.

Lin, Y.-L., Farley, R.D., Orville, H.D., 1983. Bulk parameterization of the snow field in a cloud model. J. Appl. Meteorol. Climatol. https://doi.org/10.1175/1520-0450(1983)022<1065:BPOTSF>2.0.CO;2.

Lisa, P., Christian, L., Karen, B., Blake, W., 2021. Armed conflict and cross-border asymmetries in urban development: a contextualized spatial analysis of Goma, Democratic Republic of the Congo and Gisenyi, Rwanda. Land Use Pol. 109, 105711 https://doi.org/10.1016/J.LANDUSEPOL.2021.105711.

Munro, R., Lang, R., Klaes, D., Poli, G., Retscher, C., Lindstrot, R., Huckle, R., Lacan, A., Grzegorski, M., Holdak, A., Kokhanovsky, A., Livschitz, J., Eisinger, M., 2016. The GOME-2 instrument on the Metop series of satellites: instrument design, calibration, and level 1 data processing - an overview. Atmos. Meas. Tech. 9 (3), 1279–1301. https://doi.org/10.5194/amt-9-1279-2016.

Nair, V., Hinton, G.E., 2010. A comparison of self-selected walking speeds and walking speed variability when data are collected during repeated discrete trials and during continuous walking. In: Proceedings of the 27th International Confer- Ence on Machine Learning. Israel, Haifa, 2010. https://icml.cc/Conferences/2010/papers/432.pdf.

NCEP, 2000. NCEP FNL operational model global tropospheric analyses, continuing from July 1999. In: Research Data Archive at the National Center for Atmospheric Research, Computational and Information Systems Laboratory. https://doi.org/10.5065/D6M043C6.

Nowlan, C.R., Liu, X., Chance, K., Cai, Z., Kurosu, T.P., Lee, C., Martin, R.V., 2011. Retrievals of sulfur dioxide from the Global Ozone Monitoring Experiment 2 (GOME-2) using an optimal estimation approach: algorithm and initial validation. J. Geophys. Res. Atmos. 116 (18), 1–20. https://doi.org/10.1029/2011JD015808.

Opio, R., Mugume, I., Nakatumba-Nabende, J., 2021. Understanding the trend of NO2, SO2 and CO over east Africa from 2005 to 2020. Atmosphere 12 (10). https://doi.org/10.3390/atmos12101283.

Orellano, P., Reynoso, J., Quaranta, N., 2021. Short-term exposure to sulphur dioxide (SO2) and all-cause and respiratory mortality: a systematic review and meta-analysis. Environ. Int. 150, 106434 https://doi.org/10.1016/j.envint.2021.106434.

Pouclet, A., Bram, K., 2021. Nyiragongo and Nyamuragira: a review of volcanic activity in the Kivu rift, western branch of the east african rift system. Bull. Volcanol. 83 (2) https://doi.org/10.1007/s00445-021-01435-6.

Shikwambana, L., Mhangara, P., Mbatha, N., 2020. Trend analysis and first time observations of sulphur dioxide and nitrogen dioxide in South Africa using TROPOMI/Sentinel-5 P data. Int. J. Appl. Earth Obs. Geoinf. 91, 102130 https://doi.org/10.1016/j.jag.2020.102130. March.

Skamarock, W.C., Klemp, J.B., Dudhia, J., Gill, D.O., Zhiquan, L., Berner, J., Wang, W., Powers, J.G., Duda, M.G., Barker, D.M., Huang, X.-Y., 2019. A description of the advanced Research WRF model version 4. In: NCAR Technical Note NCAR/TN-556+STR. https://doi.org/10.5065/1dfh-6p97.

Szopa, S., Naik, V., Adhikary, B., Artaxo, P., Berntsen, T., Collins, W.D., Fuzzi, S., Gallardo, L., Scharr, A.K., Klimont, Z., Liao, H., Unger, N., Zanis, P., 2021. Short-lived climate forcers. In: Masson-Delmotte, V., Zhai, A.P.P., Connors, S.L., Péan, C., Berger, S., Caud, N., Chen, Y., Goldfarb, L., Gomis, M.I., Huang, M., Leitzell, K., Lonnoy, E., Matthews, J.B.R., Maycock, T.K., Waterfield, T., Yelekçi, O., Yu, R., Zhou, B. (Eds.), Climate Change 2021: the Physical Science Basis. Contribution of Working Group I to the Sixth Assessment Report of the Intergovernmental Panel on Climate Change. Cambridge University Press. https://www.ipcc.ch/report/ar6/wg1/downloads/report/IPCC_AR6_WGI_Chapter06.pdf.

Tao, Y., Gao, X., Hsu, K., Sorooshian, S., Ihler, A., 2016. A deep neural network modeling framework to reduce bias in satellite precipitation products. J. Hydrometeorol. 17 (3), 931–945. https://doi.org/10.1175/JHM-D-15-0075.1.

Teng, J., Potter, N.J., Chiew, F.H.S., Zhang, L., Wang, B., Vaze, J., Evans, J.P., 2015. How does bias correction of regional climate model precipitation affect modelled runoff? Hydrol. Earth Syst. Sci. 19 (2), 711–728. https://doi.org/10.5194/hess-19-711-2015.

Theys, N., Hedelt, P., De Smedt, I., Lerot, C., Yu, H., Vlietinck, J., Pedergnana, M., Arellano, S., Galle, B., Fernandez, D., Carlito, C.J.M., Barrington, C., Taisne, B., Delgado-Granados, H., Loyola, D., Van Roozendael, M., 2019. Global monitoring of volcanic SO 2 degassing with unprecedented resolution from TROPOMI onboard Sentinel-5 Precursor. Sci. Rep. 9 (1), 1–10. https://doi.org/10.1038/s41598-019-39279-y.

Veefkind, J.P., Aben, I., McMullan, K., Förster, H., de Vries, J., Otter, G., Claas, J., Eskes, H.J., de Haan, J.F., Kleipool, Q., van Weele, M., Hasekamp, O., Hoogeveen, R., Landgraf, J., Snel, R., Tol, P., Ingmann, P., Voors, R., Kruizinga, B., et al., 2012. TROPOMI on the ESA Sentinel-5 Precursor: a GMES mission for global observations of the atmospheric composition for climate, air quality and ozone layer applications. Rem. Sens. Environ. 120 (2012), 70–83. https://doi.org/10.1016/j.rse.2011.09.027.

Von Schneidemesser, E., Monks, P.S., Allan, J.D., Bruhwiler, L., Forster, P., Fowler, D., Lauer, A., Morgan, W.T., Paasonen, P., Righi, M., Sindelarova, K., Sutton, M.A., 2015. Chemistry and the linkages between air quality and climate change. Chem. Rev. 115 (10), 3856–3897. https://doi.org/10.1021/acs.chemrev.5b00089.